American College of Neuropsychopharmacology

www.nature.com/npp

ARTICLE

Check for updates

Prefrontal parvalbumin interneurons deficits mediate early emotional dysfunction in Alzheimer's disease

Shu Shu[1,2,3,4,5,8], Si-Yi Xu[1,6,8], Lei Ye[1], Yi Liu[1,2,3,4,5], Xiang Cao[1,2,3,4,5], Jun-Qiu Jia[1], Hui-Jie Bian[1,7], Ying Liu[1], Xiao-Lei Zhu[1,2,3,4,5] and Yun Xu[1,2,3,4,5]✉

Alzheimer's disease (AD) is the most common neurodegenerative disease and has an insidious onset. Exploring the characteristics and mechanism of the early symptoms of AD plays a critical role in the early diagnosis and intervention of AD. Here we found that depressive-like behavior and short-term spatial memory dysfunction appeared in APPswe/PS1dE9 mice (AD mice) as early as 9-11 weeks of age. Electrophysiological analysis revealed excitatory/inhibitory (E/I) imbalance in the prefrontal cortex (PFC). This E/I imbalance was induced by significant reduction in the number and activity of parvalbumin interneurons (PV^+ INs) in this region. Furthermore, optogenetic and chemogenetic activation of residual PV^+ INs effectively ameliorated depressive-like behavior and rescued short-term spatial memory in AD mice. These results suggest the PFC is selectively vulnerable in the early stage of AD and prefrontal PV^+ INs deficits play a key role in the occurrence and development of early symptoms of AD.

Neuropsychopharmacology (2023) 48:391–401; https://doi.org/10.1038/s41386-022-01435-w

INTRODUCTION

Alzheimer's disease (AD) is a neurodegenerative disease that progresses slowly before obvious syndromes. There is still no effective cure because of the insidious onset and the unclear mechanism of the disease. Therefore, strategies for the early diagnosis and intervention to delay or prevent the development of AD may be feasible. Cognitive impairment is one of the most typical characteristics of AD, which is often initially exhibited as short-term memory problems in the preclinical stage and then shows serious long-term memory decline with disease progression [1]. Depression is also generally observed in preclinical AD, which is understood to be a risk factor for AD [2, 3]. Accumulating evidence from patients and animal models has implicated the involvement of prefrontal cortex (PFC) dysfunction in the progression of AD [4–6]. The PFC is strongly linked to cognitive function and emotion, and PFC impairment causes depressive-like behavior and cognitive deficits [7, 8]. However, it is still unclear whether and how PFC microcircuits are impaired in the incipient stage during the AD development.

It is believed that the balance between excitatory and inhibitory networks (E/I balance) is a prerequisite for the normal physiological functions in brain [9]. Current evidence demonstrates that E/I imbalance, which represents instability of glutamatergic and gamma-aminobutyric acid (GABA)ergic synaptic inputs, is the underlying cause of brain dysfunction in AD [10, 11]. Typically, abnormal elevation of glutamatergic transmission is considered a critical cause of E/I imbalance in AD pathogenesis [12, 13]. Although aberrant GABAergic transmission was observed in hippocampal circuits of AD mice, it was considered a compensatory alternation in response to glutamatergic impairment at the beginning [14]. Recently, however, increasing evidence has shown that AD patients and AD animal models with memory and cognitive impairments exhibit hippocampal neurons hyperactivity caused by GABAergic interneurons (INs) dysfunction [15–17]. Therefore, inhibitory network impairment has been gradually indicated as potential causes in early AD pathogenesis. Parvalbumin INs (PV^+ INs), accounting for ~40% of GABAergic INs in the cerebral cortex, play an important role in controlling the firing of pyramidal neurons, which they synapse onto, and orchestrating the E/I balance within PFC microcircuits and excitatory projection outputs to other regions [18, 19]. PV^+ INs dysfunction has previously been associated with AD in hippocampal-associated networks [20–22]. Although increasing attention has been given to investigating the role of GABAergic INs dysfunction in AD pathogenesis, the role of GABAergic transmission and microcircuits in the early stage of AD and the mechanisms of functional impairment mediated by GABAergic INs, especially PV^+ INs, remain unclear.

Transgenic animal models for AD have facilitated research on the pathogenesis of AD. In this study, we investigated the role of PV^+ INs in the PFC in the early stage of AD using APPswe/PS1dE9 mice (AD mice, 9–11 weeks of age). This model produces elevated levels of human Aβ by expressing mutant human APP and PS1, which is known to develop AD-like phenotypes from 5 months of age [23]. Prelimbic cortex (PrL) and infralimbic cortex (IL) are main

[1]Department of Neurology, Drum Tower Hospital, Medical School and The State Key Laboratory of Pharmaceutical Biotechnology, Nanjing University, Nanjing 210008 Jiangsu, PR China. [2]Institute of Brain Sciences, Nanjing University, Nanjing 210093 Jiangsu, PR China. [3]Jiangsu Key Laboratory for Molecular Medicine, Medical School of Nanjing University, Nanjing 210008 Jiangsu, PR China. [4]Jiangsu Province Stroke Center for Diagnosis and Therapy, Nanjing 210008 Jiangsu, PR China. [5]Nanjing Neuropsychiatry Clinic Medical Center, Nanjing 210008 Jiangsu, PR China. [6]Nanjing Drum Tower Hospital Clinical College of Jiangsu University, Zhenjiang 212013 Jiangsu, PR China. [7]Nanjing Drum Tower Hospital Clinical College of Nanjing University of Chinese Medicine, Nanjing 210023 Jiangsu, PR China. [8]These authors contributed equally: Shu Shu, Si-Yi Xu.
✉email: xuyun20042001@aliyun.com

Received: 7 April 2022 Revised: 19 July 2022 Accepted: 16 August 2022
Published online: 13 October 2022

PFC sub-regions of mice. It has been shown that PrL is closely implicated in working memory and emotional behavior dysfunction including depression [24, 25]. In this study, we focused on microcircuits function in PrL of PFC, including GABAergic transmission, PV^+ INs function and rescue. Our results showed that young adult AD mice displayed impairment of short-term spatial memory and depressive-like behaviors. These dysfunctions were associated with disrupted E/I balance and hyperactivation induced by reductions in GABAergic transmission and the number of PV^+ INs in the PFC. In addition, the behavioral deficits of these young AD mice could be rescued by optogenetic and chemogenetic activation of PV^+ INs in the PFC. These results indicated that PV^+ INs in the PFC were vulnerable in the early stage of AD, which occurred much earlier than hippocampal impairments, and our study provided a potential therapeutic target for early intervention of AD.

MATERIALS AND METHODS

Animals

Mice were group housed under a 12 h light/dark cycle (light from 8 a.m. to 8 p.m.) environment, with food and water available freely. Male APPswe/PS1dE9 (APP/PS1) transgenic mice and WT littermates were acquired from Nanjing Biomedical Research Institute of Nanjing University. PV-Cre mice (The Jackson Laboratory, Stock No.: 017320) were kindly obtained from Professor Ji Hu from ShanghaiTech University [26]. Homozygous PV-Cre mice were crossed with hemizygous APP/PS1 mice to produce double-transgenic PV-Cre:APP/PS1 mice and single-transgenic PV-Cre control littermates. All animal studies were approved by the Animal Care Committee of Nanjing University.

Behavioral tests

The behavioral battery used is described in Fig. S1A. The Y-maze test, open field test and Morris water maze (MWM) were performed as previously described [27, 28] to measure the short-term spatial memory, locomotor activation, anxiety-like behavior and long-term spatial memory. Nesting test, tail suspension test and sucrose preference test were used to apathy- and depressive-like behaviors. Mice were put into the room for 1 h to habituate before all behavioral tests. All behavioral tests were performed and analyzed blinded to genotype or treatments. Details for behavioral tests are included in Supplementary Materials and Methods.

Stereotaxic surgery

Mice were anesthetized by inhaling a 5% isoflurane-oxygen mixture, anesthesia was maintained with a 2–3% isoflurane-oxygen mixture during surgery. The ocular lubricant was applied to avoid drying of eyes during surgery. The mice were secured in a stereotaxic apparatus (RWD, Shenzhen, China). Holes were drilled into the skull for virus injection or electrode implantation bilaterally into PFC at coordinates (AP 2.10 mm, ML ±0.40 mm, DV 2.30 mm), or for fiber implantation bilaterally with an 10° angle at coordinates (AP 2.10 mm, ML ±0.76 mm, DV 2.03 mm). After surgery, mice were allowed 7–21 days for recovery and expression before experiments and mice implanted with electrodes or fibers were single housed.

Virus, fiber and electrode

Floxed hChR2 and control (rAAV-Ef1α-DIO-hChR2(H134R)-EYFP-WPRE-pA; rAAV-Ef1α-DIO-EYFP-WPRE-pA) AAVs (10^{12}vg/ml; serotype 2/9), floxed hM3D(Gq) and control (rAAV-Ef1a-DIO-hM3D(Gq)-EGFP-WPREs; rAAV-EF1a-DIO-EGFP-WPRE-hGH-pA) AAVs (2×10^{12}vg/ml; serotype 2/9) were purchased from BrainVTA (Wuhan, China). Fiber optic cannulas (ferrule: φ1.25 mm, fiber core: 200 μm, NA: 0.37, fiber length: 2.2 mm) were purchased from Inper (Hangzhou, China). The electrodes (16 nickel-chromium and HFV natural-insulated microwires (diameter: 25 μm, California Fine Wire, Grover Beach, CA, USA) and two uninsulated silver wires (diameter: 125 μm) as reference and ground wires, assembled in the connector) were custom-made from Hong Kong Plexon Limited (Hong Kong, China).

In vivo recording

After surgery, the mice were allowed to recover for at least 7 days before recording. Spikes and local field potential (LFP) signals were amplified; band-pass filtered (0.5–1000 Hz for LFP, 250–8000 Hz for spikes) and digitized (40 kHz) by the OmniPlex Neural Data Acquisition System (Plexon, Dallas, TX, USA). Mice's behavior was monitored throughout the behavior test (Y maze) with a digital camera right above the center of the maze, the video was recorded using CinePlex Studio software (Plexon, Dallas, TX, USA), and was simultaneously recorded with electrophysiological data.

Power analysis, spike sorting and analysis

LFP recordings were processed in Neuroexplorer (Nex Technologies, Madison, AL, USA). Power spectrum data were calculated by normalizing auto-spectrum products so that the values are equal to the mean squared values from the rate histogram that were calculated from the overall data. Normalized data was then converted to logarithmic scale and filtered by Gaussian filter with bin size of 1 [29]. Spike sorting was performed offline with Offline Spike Sorter software (Plexon, Dallas, TX, USA). Principal component analysis was applied to separate waveforms into individual clusters, automatically. The isolation distance and L-ratio was calculated to estimate the quality of cluster separation. The units were included in the data analysis in the condition of well-isolated (L-ration less than 0.2 and distance lager than 15). Spikes in pyramidal neurons (PNs) were identified and distinguished from interneurons (INs) based on the duration of the negative spike, the firing pattern and the low firing rate. The average firing rates were calculated as the total number of spikes divided by the total length of recording period.

Slice preparation and in vitro electrophysiology

Acute slices (300 μm) were prepared as previously described [27]. Details for PFC slice preparation and whole-cell patch clamp recordings are included in Supplementary Materials and Methods.

In vivo microdialysis and neurotransmitter measurement

After anesthetized with an isoflurane-oxygen mixture, the mice were secured in a stereotaxic apparatus (RWD, Shenzhen, China). The CMA7 microdialysis probe (ITEM # P000082, membrane length: 1 mm) of concentric design (CMA, Solna, Sweden) was inserted into PFC at coordinates (AP 2.10 mm, ML ±0.40 mm, DV 2.30 mm). The probe was connected to a 1 ml microsyringe (CMA, Solna, Sweden) perfused with ACSF and controlled by a microperfusion pump (Harvard Apparatus, USA) at a speed of 2 μl/min. The outlet perfusates were collected in 1.5 ml EP tubes standing in ice. The perfusates which collected after perfusing 20 min were used for measurement. The GABA and glutamate levels were measured via HPLC-MS/MS, which performed by Experimental Research Center, China Academy of Chinese Medical Sciences (Beijing, China).

Optogenetic stimulation

For in vivo optogenetic stimulating PV^+ INs, light pulses were generated using a 465-nm wavelength via laser Smart Light Souse (Inper, Hangzhou, China) controlled via Inper Studio software (Inper, Hangzhou China). The laser power was regulated depending on the penetration rate of the fiber, and the final laser power at fiber tip was 0.5–1.5 mW/mm^2, the blue light (465 nm) was delivered at 40 Hz (1 s on, 10 s off) during behavioral tests (Y maze test and TST). In Y maze test, the light was delivered for 1 s before mice entering center zone manually. In SPT, the light was delivered 1 h before test (40 Hz, 1 s on, 10 s off, lasted for 1 h). Data of light on and light off within the same animal were compared.

Chemogenetic stimulation

Clozapine N-oxide (CNO) was purchased from BrainVTA (Wuhan, China). CNO was dissolved in sterile 0.9% saline and kept at −20 °C before administration. In Y maze test and TST, CNO was given at a dose of 1 mg/kg through intraperitoneal injection 30 min before test. In SPT, besides intraperitoneal injection 30 min before test, the CNO was also administrated in both water and sucrose bottles (5 μg/ml). Mice weighed 20–25 g and consumed ~5 ml/day for a long-lasting chemogenetic activation.

Tissue preparation and immunofluorescence

Immunofluorescence for brain sections was performed as previously described [28]. Details for tissue preparation, staining, image acquisition, analysis and antibodies are included in Supplementary Materials and Methods.

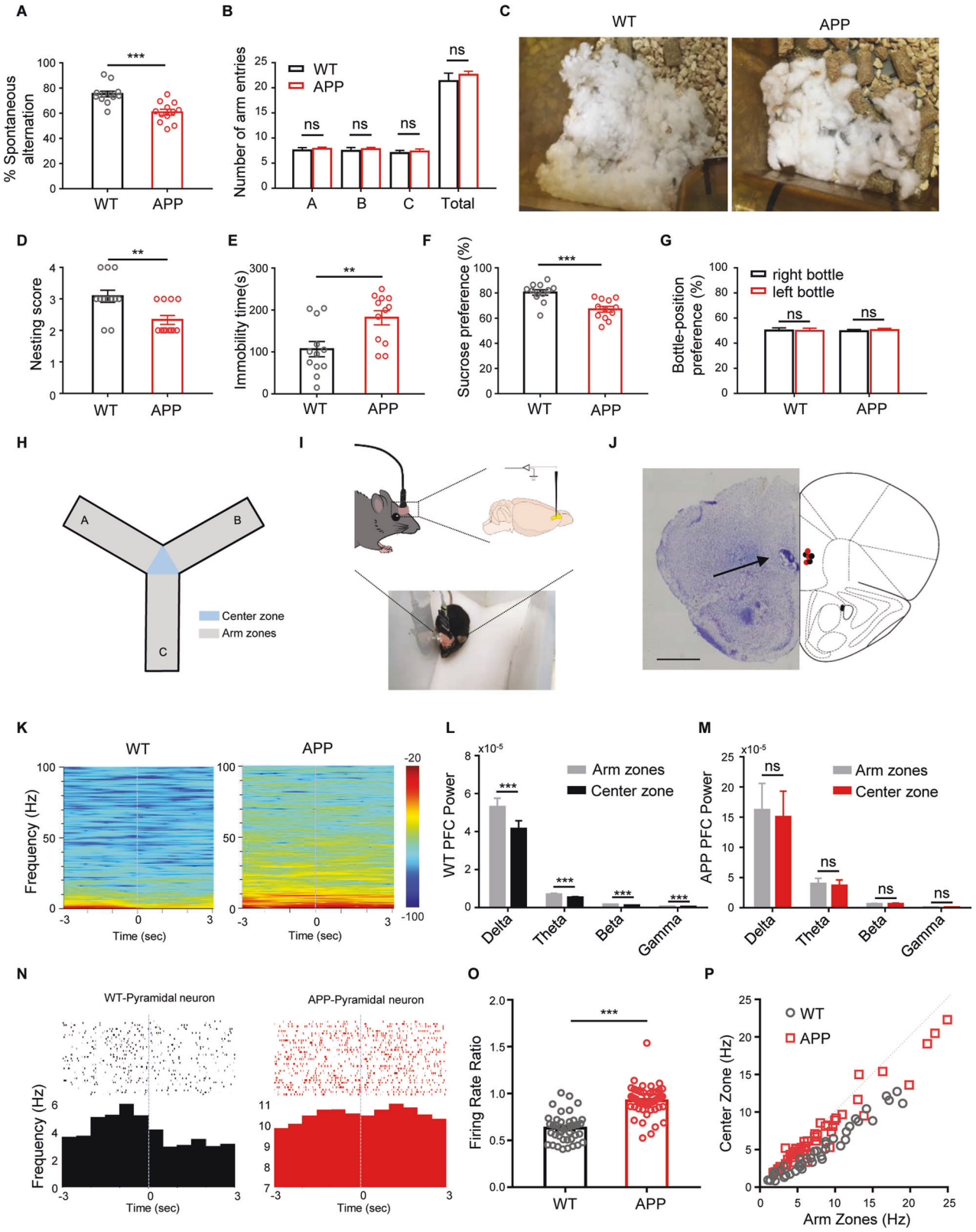

RT-PCR

PFC tissues were separated and collected after vibrating sectioning (4 °C). Details for total RNA isolation, reverse transcription, RT-PCR and primers are included in Supplementary Materials and Methods.

Western blot

PFC tissues were separated and collected after vibrating sectioning (4 °C) and then prepared protein lysates using RIPA buffer (Thermo, Pittsburgh, PA, USA) containing phosphatase and protease inhibitors. Tissue lysate was

Fig. 1 Short-term memory impairment and depressive-like behaviors in young adult AD mice and lack of necessary silencing during short-term memory tasks. **A** Reduced spontaneous alternation percentage in APP mice. $t(22) = 4.42$, $p = 0.0002$. **B** APP and WT mice made similar number of entries into each arm and total arms. $t(22) = 0.53$, $p = 0.5985$ for **A**; $t(22) = 0.54$, $p = 0.5979$ for **B**; $t(22) = 0.45$, $p = 0.6604$ for **C**; $t(22) = 0.84$, $p = 0.4101$ for Total. **C** Representative nests in the nesting test shown from the top. **D** APP mice received lower nesting scores then WT mice. $t(22) = 3.13$, $p = 0.0049$. **E** APP mice exhibited longer immobility time then control in the tail suspension test. $t(22) = 3.03$, $p = 0.0062$. **F** Decreased sucrose preference percentage of APP mice, compared with control mice. $t(22) = 4.23$, $p = 0.0003$. **G** No preference of bottle-position of APP or WT mice in SPT. $t(22) = 0.08$, $p = 0.9380$ for WT; $t(22) = 0.44$, $p = 0.6641$ for APP. **H** Schematic diagram of the Y-maze with arm zone and center zone. **I** Photograph of a mouse subjected to the Y-maze for in vivo recording (bottom) and enlargement illustration multichannel electrode implantation (top). **J** Left: electrode placements in control mice (black circle) and APP mice (red circle) in the prefrontal cortex. Right: location of electrode tips in the PFC. Nissl staining image shows lesions made by electronic heat (arrow). Scale bar: 1 mm. **K** Representative local field potential (LFP) spectrogram of the PFC during mice entering the center zone (time 0). **L** Decreased mean LFP power in different bands of WT mice PFC ($n = 3$ mice) after mice entered the center zone, compared with mice in the arm zones. $t(27) = 4.40$, $p = 0.0002$ for Delta; $t(27) = 5.13$, $p < 0.0001$ for Theta; $t(27) = 5.09$, $p < 0.0001$ for Beta; $t(27) = 7.50$, $p < 0.0001$ for Gamma. **M** Comparable mean LFP power in different bands of APP mice PFC ($n = 3$ mice) after mice entering center zone and in the arm zones. $t(31) = 1.78$, $p = 0.0844$ for Delta; $t(31) = 1.67$, $p = 0.1051$ for Theta; $t(31) = 1.58$, $p = 0.1239$ for Beta; $t(31) = 1.71$, $p = 0.0976$ for Gamma. **N** Representative raster plot (top) and peri-stimulus time histogram (PSTH; bottom) of PFC pyramidal neurons from WT and APP mice when they entered the center zone (time 0). **O** Increased PFC pyramidal neurons firing ratio (the firing rate within 3-s period after mice entered the center zone divided by the firing rate within the 3-s period before mice entered the center zone) of APP mice ($n = 52$ units, 3 mice), compared with WT mice ($n = 40$ units, 3 mice). $t(90) = 9.01$, $p < 0.0001$. **P** Correlation of firing rate of individual PFC pyramidal neurons at baseline (3 s before mice entered the center zone) and in the 3-s period after the mice entered the center zone. Data were shown as mean ± SEM, $n = 12$ mice in **A**, **B**, **D**–**G**. Unpaired two-tailed *t*-test for **A**, **B**, **D**–**G** and **O**. Paired two-tailed *t*-test for **L** and **M**. $^{**}p < 0.01$, $^{***}p < 0.001$; ns no significance.

subjected to western blotting as previously described [28]. Details for tissue preparation, western blotting, analysis and antibodies are included in Supplementary Materials and Methods.

Statistical analysis

All data values in the text and figure legends are represented as the mean ± standard error of the mean. Statistical analyses were performed by GraphPad Prism 7. Differences between groups were assessed using *t*-tests, one- or two-way analysis of variance, which were indicated in the figure legends. A statistically significant difference was set at $p < 0.05$.

RESULTS

Short-term memory impairment and depressive-like behaviors in young adult AD mice

To detect phenotypes in the early stage of AD, the 9- to 11-week-old APPswe/PS1dE9 (APP/PS1) mice were subjected to the Y-maze (Fig. 1A, B) and the MWM test (Fig. S1B–G) for the evaluation of short-term working memory and long-term spatial learning and memory, separately. In the Y-maze test, APP/PS1 mice made fewer spontaneous alterations than control mice (Fig. 1A), suggesting a significant impairment of short-term memory in mice in the early stage of AD. However, in the training session of the MWM test, the young adult APP/PS1 mice showed a similar latency to reach the hidden platform as control (Fig. S1B). During the probe test, the swimming speed, latency to first entry into the platform location, number of platform location crossings and time spent in the target quadrant were similar between groups (Fig. S1C–G). These results suggest that young adult AD mice exhibited short-term but not long-term memory impairment.

To determine whether young adult AD mice display emotional disorders, the mice were subjected to the open field test, nesting test, tail suspension test and sucrose preference test (Figs. S1H–J and 1D–G). In the open field test, APP/PS1 mice spent a similar amount of time in the center zone as WT mice, and there was no significant difference in mean speed between the two groups (Fig. S1H–J). In the nesting behavior test, APP/PS1 mice built lower-scoring nests than littermate controls (Fig. 1C, D). In the tail suspension test and sucrose preference test, APP/PS1 mice displayed a significant increase in immobility time and an obvious decrease in sucrose intake (%) compared with WT mice (Fig. 1E–G). These results indicate that young adult AD mice showed significant negative emotions (depressive-like and apathy-like behaviors but not anxiety-like behavior) in addition to short-term spatial memory impairment.

Lack of necessary silencing in the PFC of young adult AD mice during short-term memory tasks

Since the PFC is involved in short-term memory and emotional disorders, we thus investigated whether the PFC performed abnormal functions during short-term working memory tasks by in vivo recordings from freely moving APP/PS1 mice in a Y maze (Fig. 1H–J). We focused on neuronal activity in the PFC (LFPs and spikes) when mice entered the center zone of the maze, which was essential for mice to choose the next arm zone during short-term spatial memory (Fig. 1H). Neuronal activity in the 3-s period before and 3-s period after the mice entered the center zone was analyzed. Analysis of LFP showed that the power was significantly decreased in each band (delta: 0.5–4 Hz; theta: 4–12 Hz; beta: 12–30 Hz; gamma: 30–100 Hz) when WT mice entered the center zone (Fig. 1K, L). However, this reduction in LFP power in the PFC was absent in young AD mice (Fig. 1K, M). Furthermore, the spiking activity (firing rate) of PFC pyramidal neurons was decreased when WT mice, but not young AD mice, entered the center zone (Fig. 1N–P). These results suggested that the necessary silencing of neuronal activity in the PFC was impaired in young adult APP/PS1 mice during short-term memory tasks.

Increased network excitability of pyramidal neurons and E/I imbalance in the PFC

Furthermore, in vivo recordings were obtained from freely moving APP and WT mice in their home cages (Fig. 2A). The results indicated that the firing rates of pyramidal neurons and power of LFP in each band in the PFC were increased in APP mice compared with controls (Figs. 2B, C and S2). Consistently, the in vitro electrophysiology results showed that in the absence of CNQX, D-APV and bicuculline, the RMP and AP frequency were significantly increased in response to current injection, and the AP threshold in response to injected current was reduced for PFC pyramidal neurons in young adult AD mice, compared with control mice (Fig. 2D–G). The input resistance was not different in PFC pyramidal neurons between young AD mice and littermate controls (Fig. 2H, L). However, when excitatory and inhibitory neurotransmissions were pharmalogically blocked, the firing frequency and action potential (AP) threshold were similar between the two groups of mice (Fig. 2I–K). In addition, the E/I balance was also measured in the PFC and the results showed that E/I ratio was higher in AD mice, compared with littermates (Fig. 2M, N). Together, these results indicated that the network excitability but not the inherent excitability of pyramidal neurons was significantly increased and the E/I balance was altered in the PFC of young adult AD mice.

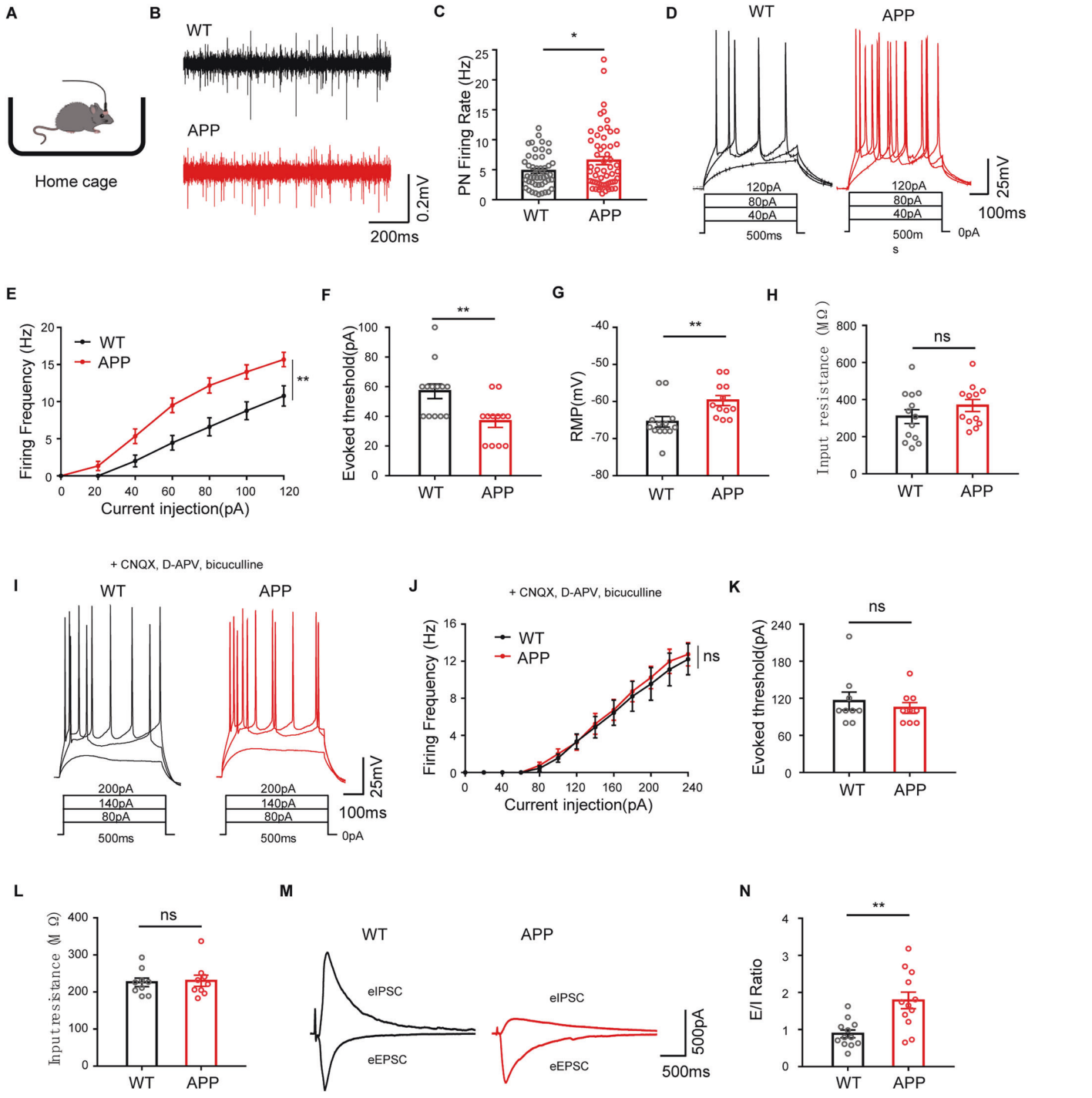

Decreased GABAergic transmission in the PFC of young adult AD mice

Elevated neuronal activity might be caused by increased excitatory inputs, decreased inhibitory inputs or both, which indicates E/I imbalance [20]. To investigate whether glutamatergic transmission is altered in young adult APP/PS1 mice, we measured miniature excitatory postsynaptic currents (mEPSCs) in PFC pyramidal neurons (Fig. S3). The frequency and amplitude of mEPSCs were similar between APP mice and control littermates (Fig. S3A–D), indicating normal glutamatergic transmission. Analysis of miniature inhibitory postsynaptic currents (mIPSCs) revealed a significant reduction in mIPSC frequency but not amplitude in PFC pyramidal neurons in young adult APP mice compared with WT controls (Fig. 3A–D). Furthermore, the paired-pulse ratio was dramatically increased in APP mice (Fig. 3E, F), indicating that GABA release from interneurons decreased. We thus measured the extracellular concentration of GABA in the PFC using HPLC-MS/MS analysis. The interstitial fluid samples from the PFC were collected from the two groups by microdialysis (Fig. 3G). Consistently, the results indicated a significant decrease in GABA levels but not glutamate levels in the PFC of young adult APP mice compared with the PFC of WT littermates (Fig. 3H, I). We also detected mIPSCs in pyramidal neurons in the hippocampal CA1 region, one of the most vulnerable regions in AD [17, 20], in age-matched APP mice (Fig. S4); however, the frequency and amplitude of

Fig. 2 Increased network excitability of pyramidal neurons and E/I imbalance in the PFC of young adult AD mice. A Schematic illustration of an in vivo recording from a mouse in home cage. **B** Representative recording traces of action potentials (APs) in PFC pyramidal neurons. **C** Increased firing rate of PFC pyramidal neurons of APP mice ($n = 57$ units, 3 mice), compared with WT mice ($n = 48$ units, 3 mice). $t(103) = 2.09$, $p = 0.0395$. **D–F** Increased network excitability of pyramidal neurons in PFC of young adult AD mice. **D** Representative AP traces of spikes evoked by injecting depolarizing currents in absence of CNQX, D-APV and bicuculline. **E** Increased average AP frequency of PFC pyramidal neurons in response to 0- to 120-pA depolarizing current steps in APP mice ($n = 12$ neurons, 3 mice), compared with WT mice ($n = 13$ neurons, 3 mice). $F(1, 23) = 12.71$, $p = 0.0016$. **F** Reduced injected current required to evoke AP (evoked threshold) of PFC pyramidal neurons of APP mice ($n = 12$ neurons, 3 mice), compared with WT mice ($n = 13$ neurons, 3 mice). $t(23) = 3.10$, $p = 0.0051$. **G** Increased rest membrane potential (RMP) of PFC pyramidal neurons of APP mice ($n = 12$ neurons, 3 mice), compared with WT mice ($n = 13$ neurons, 3 mice). $t(23) = 2.89$, $p = 0.0082$. **H** Comparable input resistance of PFC pyramidal neurons of APP mice ($n = 12$ neurons, 3 mice) and WT mice ($n = 13$ neurons, 3 mice). $t(23) = 1.19$, $p = 0.2456$. **I–K** No change in intrinsic excitability of pyramidal neurons in the PFC of young adult AD mice. **I** Representative AP traces of spikes evoked by injecting depolarizing currents. **J** Similar average AP frequency of PFC pyramidal neurons in response to 0- to 240-pA depolarizing current steps between APP mice ($n = 9$ neurons, 3 mice) and WT mice ($n = 9$ neurons, 3 mice). $F(1, 15) = 0.09$, $p = 0.7655$. **K** Comparable injected current required to evoke AP (evoked threshold) of PFC pyramidal neurons of APP mice ($n = 9$ neurons, 3 mice), compared with WT mice ($n = 9$ neurons, 3 mice). $t(16) = 0.66$, $p = 0.5190$. **L** Comparable input resistance of PFC pyramidal neurons of APP mice ($n = 9$ neurons, 3 mice) and WT mice ($n = 9$ neurons, 3 mice) with excitatory and inhibitory neurotransmissions pharmalogically blocked. $t(16) = 0.22$, $p = 0.8309$. **M** Representative eEPSC and eIPSC trace. **N** Increased excitatory/inhibitory (E/I) ratio in APP mice ($n = 12$ neurons, 3 mice), compared with WT mice ($n = 12$ neurons, 3 mice). The E/I ratio was calculated as amplitude (averaged eEPSC)/amplitude (averaged eIPSC). $t(22) = 3.66$, $p = 0.0014$. Data were shown as mean ± SEM. Unpaired two-tailed *t*-test for **C**, **F–H**, **K**, **L** and **N**. Two-way ANOVA followed by Bonferroni's post hoc test for **E** and **J**. $^*p < 0.05$, $^{**}p < 0.01$; ns no significance.

mIPSCs were similar between slices from the two groups (Fig. S4A–D). These results suggested that GABAergic transmission was impaired in the PFC of young adult APP mice. These results indicated a significant reduction in GABA transmission in the PFC but not the CA1 region in young AD mice.

In addition, we observed an obvious change in mIPSCs kinetics (Fig. S5A). mIPSCs in pyramidal neurons in the PFC exhibited slower decay kinetics but a similar rise time in AD mice compared with WT littermates (Fig. S5A–D). This slower mIPSC kinetics might be associated with changes in the density of $GABA_A$ receptor subunits [30]. To address the cause of this kinetics change, the mRNA expression of $GABA_A$ receptor α1-3 subunits was detected. The RT-PCR results indicated that the mRNA expression of α1 subunit was decreased, α2 subunit has no marked change and α3 subunit has an increasing trend with no significant difference in the PFC in AD mice, compared with WT controls (Fig. S5E). These results suggested that mIPSC decay kinetics were significantly reduced in the PFC of young AD mice and this reduction might have been due to alternations in proportions of α1-3 subunits, especially α1 subunit of $GABA_A$ receptor.

Decreased PV^+ cell number and activity in the PFC of young adult AD mice

To investigate the potential mechanism by which GABA release is reduced, we measured the levels of proteins that are essential for GABA synthesis and transport. The Western blot results showed that the protein expression levels of GAD65/67 and VGAT in the PFC were similar between APP and WT mice (Fig. S5F), indicating normal GABA synthesis and transport in young adult AD mice.

GABAergic INs supply inhibitory terminals, GABA is released onto pyramidal neurons in the cortex, and loss of GABAergic INs leads to a reduction in GABA transmission [31]. To determine whether the number of INs was altered in the PFC in young AD mice, the levels of somatostatin (SOM) and parvalbumin (PV), markers of the two main IN classes (somatostatin interneurons (SOM^+ INs): 20–30% of INs, PV^+ INs: 40–50% of INs) in the PFC [32], were measured. The immunofluorescence results showed that the number of PV^+ INs, but not SOM^+ INs, in the PFC was significantly decreased in young adult AD mice compared with WT littermates (Fig. 4A–F) and there were a small number of amyloid plaques in the PFC in AD mice (Fig. S6A–C, F). Meanwhile, the number of PV^+ INs and SOM^+ INs in the hippocampus were not altered in AD mice compared with controls (Fig. S7A–D) and no amyloid plaque was detected in the hippocampus in AD mice (Fig. S6D, E).

Then, we determined whether the neuronal properties of PV^+ INs were altered in the PFC of young AD mice. For PV^+ INs whole-cell recordings (in layer V), we used PV:APP mice and PV:WT littermate control mice (Fig. 5A) which were bilaterally injected rAAV-EF1α-DIO-EYFP in the PFC. The EYFP-positive neurons were identified as PV^+ INs. The in vitro electrophysiology results showed that the input resistance of PFC PV^+ INs was similar between the two groups but the RMP and AP frequency in response to current injection were decreased in PFC PV^+ INs in young adult APP/PS1 mice compared with control mice (Fig. 4G–K). These results indicated that the number and activity of PV^+ cells were both decreased in the PFC in young AD mice.

Increased activity of PV^+ INs rescued short-term spatial memory and ameliorated depressive-like behavior

It remains unclear whether this decrease in PV^+ IN neuronal activity and the imbalance of PFC microcircuits causes short-term memory deficits and depressive-like behaviors in young adult APP/PS1 mice. To address this, we increased activity of PV^+ INs in PFC by optogenetics or chemogenetics and evaluated cognitive and emotional function of AD mice. First, we crossed APP/PS1 transgenic mice with PV-Cre mice to obtain PV:APP mice and PV:WT littermate control mice (Fig. 5A). Next, we bilaterally injected adeno-associated virus (AAV) carrying double-floxed channelrhodopsin-2 (ChR2) or control AAV, implanted optical fibers into the PFC and performed behavioral tests on these two groups of mice (Figs. 5B, C and S8A, B). The in vitro electrophysiology results showed that blue-light activation of ChR2-expressing PV^+ INs in the PFC immediately caused AP bursts (Fig. S8C, D), and the network excitability of pyramidal neurons in the PFC of PV:APP mice was inhibited effectively (Fig. S8E–G). Optogenetic activation of PV^+ INs in the PFC rescued the reduction in spontaneous alternation percentage in the Y-maze test, the increase in immobility time in the tail suspension test and the decrease in sucrose preference percentage in the sucrose preference test in PV:APP mice (Fig. 5D–G). In addition, we bilaterally injected AAV carrying hM3D(Gq) or control AAV and performed behavioral tests on PV:APP and PV:WT mice (Figs. 5H, I and S9A, B). The in vitro electrophysiology results showed that administration of clozapine N-oxide (CNO) could evoke hM3D(Gq) expressing PV^+ INs in the PFC firing successfully (Fig. S9C, D). Furthermore, the network excitability of pyramidal neurons in the PFC of PV:APP mice was decreased significantly (Fig. S9E–G). Consistently, the behavior test results showed that chemogenetic activation of PV^+ INs in the PFC rescued the reduction in spontaneous alternation percentage in the Y-maze test, the increase in immobility time in the tail suspension test and the decrease in sucrose preference percentage in the sucrose preference test in PV:APP mice (Fig. 5J–L). These results suggested that an acute increase in PV^+ INs activity in the PFC was sufficient to rescue short-term spatial memory and ameliorate depressive-like behavior in young adult AD mice.

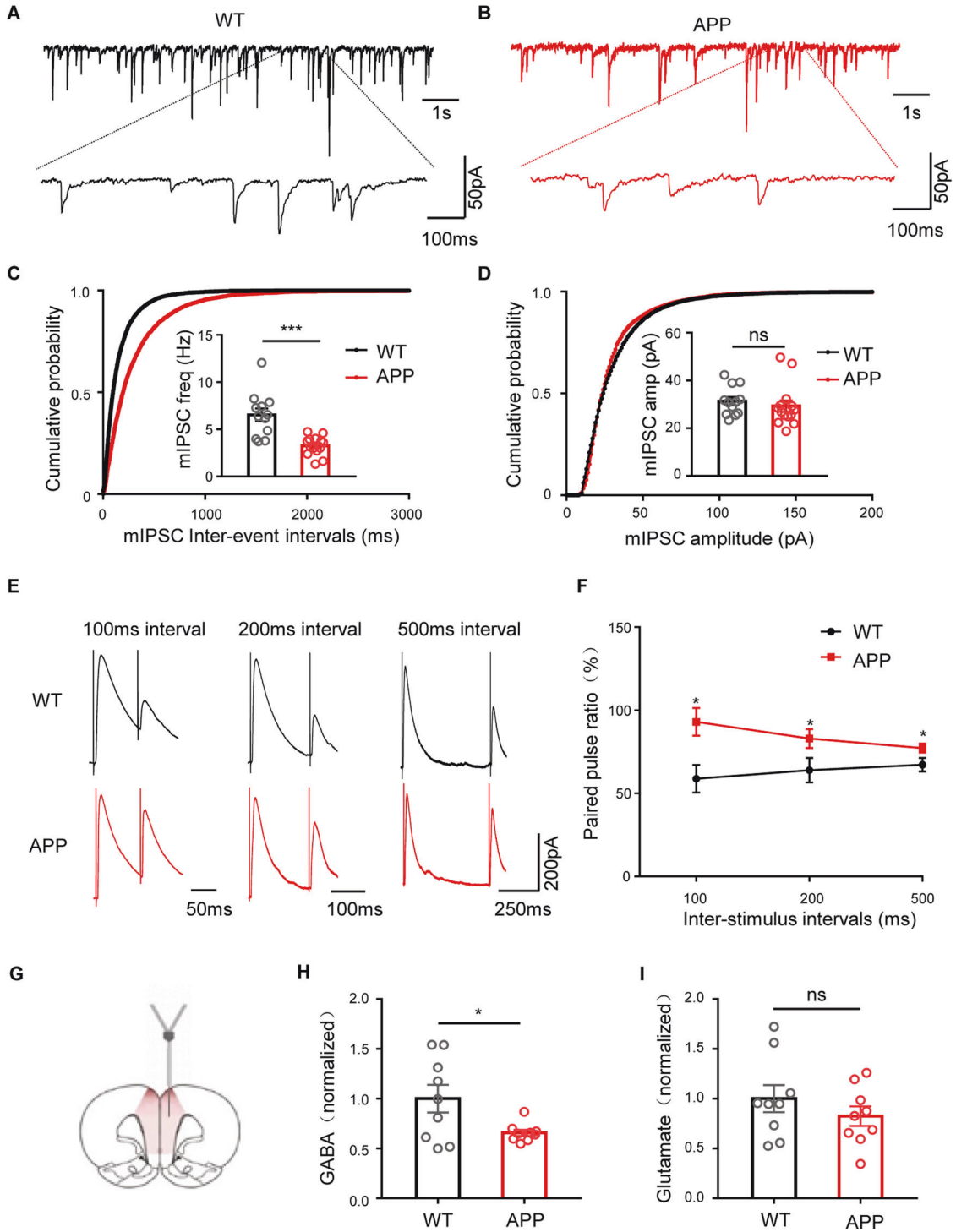

Fig. 3 Decreased GABAergic transmission in the PFC of young adult AD mice. A, **B** Representative traces of mIPSC in PFC pyramidal neurons of WT and APP mice. **C** Decreased mIPSC frequency of PFC pyramidal neurons of APP mice ($n = 14$ neurons, 3 mice), compared with WT mice ($n = 12$ neurons, 3 mice). $t(24) = 4.70$, $p < 0.0001$. **D** Comparable mIPSC amplitude of pyramidal neurons of PFC in APP mice ($n = 14$ neurons, 3 mice) and WT mice ($n = 12$ neurons, 3 mice). $t(24) = 0.69$, $p = 0.4971$. **E** Representative traces of pair-pulse stimulation. **F** Paired-pulse ratio (PPR) plotted against inter-stimulus intervals. $F\ (1, 16) = 8.94$, $p = 0.0087$. **G** Schematic diagram showing in vivo microdialysis. **H** Decreased GABA levels in the PFC of APP mice ($n = 9$), compared with WT mice ($n = 9$). $t(16) = 2.42$, $p = 0.0279$. **I** Comparable glutamate levels in the PFC of APP mice ($n = 9$) and WT mice ($n = 9$). $t(16) = 1.05$, $p = 0.3102$. Data were shown as mean ± SEM. Unpaired two-tailed *t*-test for **C**, **D**, **H** and **I**. Two-way ANOVA followed by Bonferroni's post hoc test for **F**. *$p < 0.05$, **$p < 0.01$, ***$p < 0.001$; ns no significance.

Taken together, our results suggest that defective PV^+ INs in PFC microcircuits in young adult AD mice might result in short-term spatial memory impairment and depressive-like behavior by triggering GABA transmission deficits and E/I imbalance.

DISCUSSION

The main goal of this study was to explore the cognitive and emotional symptoms in the early stage of AD and investigate the underlying mechanism. The major findings of this paper are as

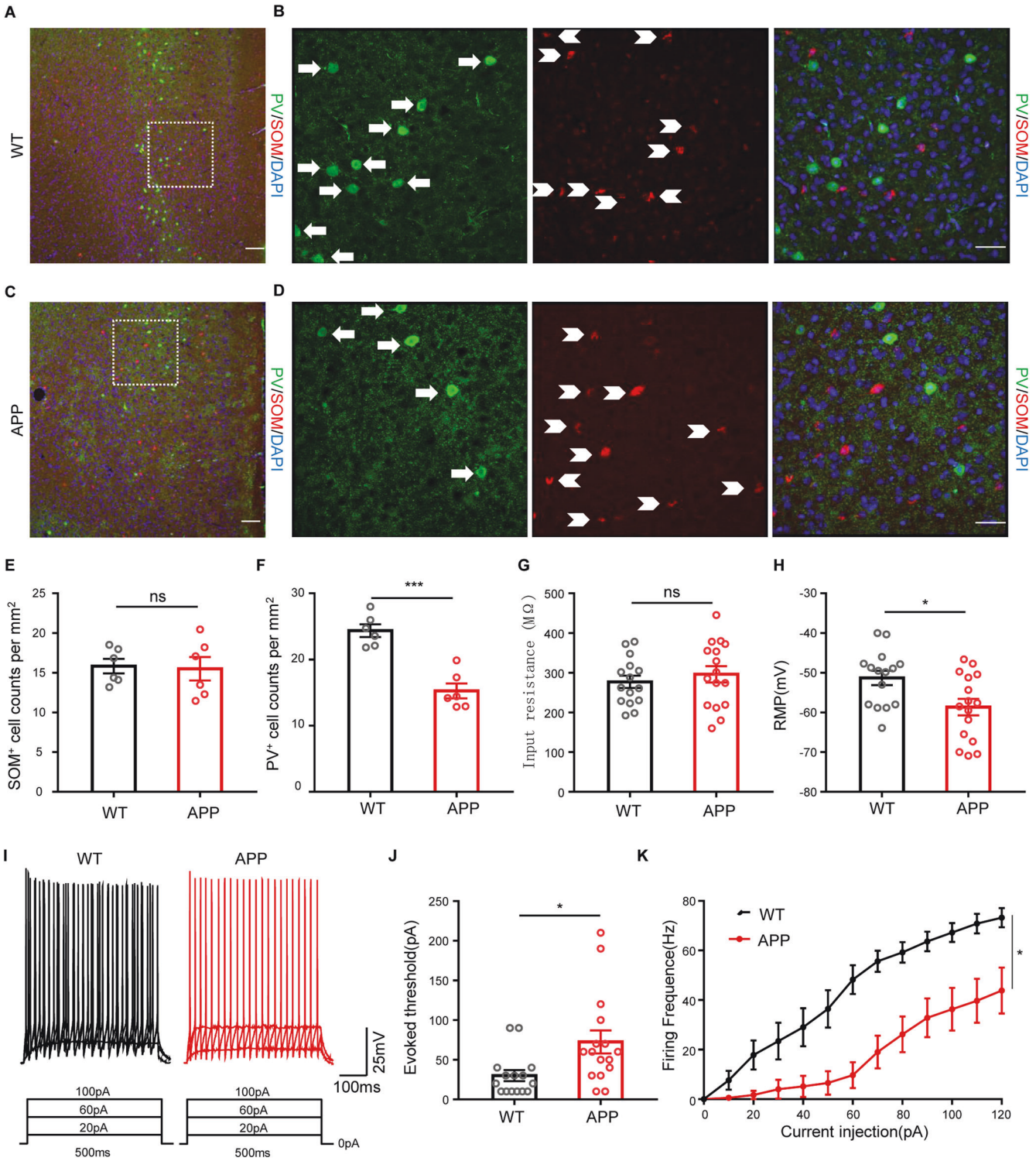

Fig. 4 Decreased PV$^+$ cell number and activity in the PFC of young adult AD mice. Representative fluorescence images (**A**) and enlargement (**B**) showing the PV$^+$ INs (green) and SOM$^+$ INs (red) in PFC of WT mice. Scale bar: 100 μm. Representative fluorescence images (**C**) and enlargement (**D**) showing the PV$^+$ INs (green) and SOM$^+$ INs (red) in PFC of APP mice. Scale bar: 100 μm. **E** Comparable number of SOM$^+$ INs in the PFC of APP mice ($n = 6$ mice) and WT mice ($n = 6$ mice). $t(10) = 0.20$, $p = 0.8516$. **F** Reduced number of PV$^+$ INs in the PFC of APP mice ($n = 6$ mice), compared with WT mice ($n = 6$ mice). $t(10) = 6.12$, $p = 0.0001$. **G** Comparable input resistance of PFC PV$^+$ INs of APP mice ($n = 16$ neurons, 3 mice) and WT mice ($n = 15$ neurons, 3 mice). $t(29) = 0.73$, $p = 0.4688$. **H** Decreased rest membrane potential (RMP) of PFC PV$^+$ INs of APP mice ($n = 16$ neurons, 3 mice), compared with WT mice ($n = 15$ neurons, 3 mice). $t(29) = 2.66$, $p = 0.0126$. **I** Representative AP traces of spikes evoked by injecting depolarizing currents. **J** Increased injected current required to evoke APs (evoked threshold) of PFC PV$^+$ INs of APP mice ($n = 16$ neurons, 3 mice), compared with WT mice ($n = 15$ neurons, 3 mice). $t(29) = 2.61$, $p = 0.0143$. **K** Decreased average AP frequency of PFC PV$^+$ INs in response to 0- to 120-pA depolarizing current steps in APP mice ($n = 16$ neurons, 3 mice), compared with WT mice ($n = 15$ neurons, 3 mice). $F(1, 22) = 14.63$, $p = 0.0009$. Data were shown as mean ± SEM. Unpaired two-tailed *t*-test for **E**–**H** and **J**. Two-way ANOVA followed by Bonferroni's post hoc test for **K**. *$p < 0.05$, ***$p < 0.001$; ns no significance.

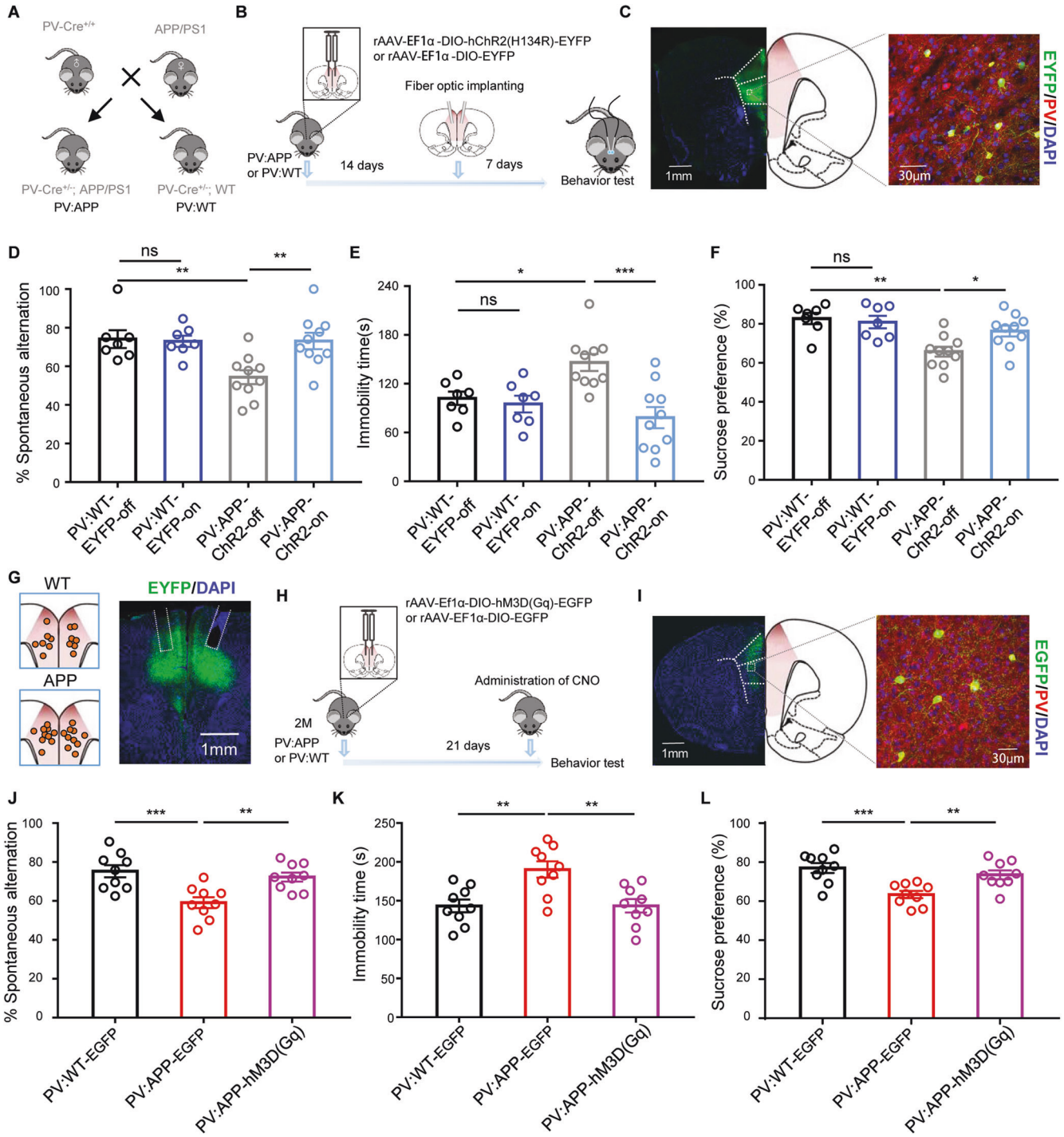

follows. First, APP/PS1 mice exhibited short-term spatial memory impairment and depressive-like behavior but not long-term spatial learning and memory impairment at 9–11 weeks of age (the early stage of AD). The network excitability of pyramidal neurons in the PFC was increased in APP mice. Necessary silencing in the PFC during short-term memory tasks was impaired in young AD mice. Second, we found that GABAergic but not glutamatergic transmission was decreased in the PFC, but it was not reduced in the hippocampal CA1 region in young AD mice. This reduction was associated with decreases in PV^+ INs activity and number. Third, an optogenetic or chemogenetic-induced increase in the activity of PV^+ INs rescued impaired short-term memory and ameliorated depressive-like behavior. Altogether, these results suggest that emotional and short-term cognitive dysfunctions occur at an early stage of AD. These dysfunctions are associated with PFC GABAergic transmission impairment and E/I imbalance, which are induced by PV^+ IN deficits.

Excitatory and inhibitory neurons coactivate in the normal brain and maintain normal network activities, while this E/I balance is disrupted in AD [33]. Synaptic plasticity plays an important role in maintaining network E/I balance. Both excitatory and inhibitory synapses are modulated by short-term plasticity, potentially causing dynamic modulation of the E/I ratio [34]. Impaired homeostatic synaptic plasticity may cause significant alteration in the synaptic E/I

Fig. 5 Increased activity of PV$^+$ INs rescued short-term spatial memory and ameliorated depressive-like behavior. A Schematic diagram of breeding strategy to generate PV:APP mice and PV:WT mice. **B** Schedule and diagram for the optogenetics experiment. **C** Representative image of viral transduction and a close-up showing EYFP-positive neurons were highly localized in PV$^+$ neurons. **D** Spontaneous alternation percentage in the Y-maze test upon optogenetic activation, $n = 10$ for PV:APP mice, $n = 7$ for PV:WT mice. F (3, 30) = 6.36, WT-off vs. WT-on: $p = 0.9977$, WT-off vs. APP-off: $p = 0.0084$, APP-off vs. APP-on: $p = 0.0055$. **E** Immobility time in the tail suspension test upon optogenetic activation, $n = 10$ for PV:APP mice, $n = 7$ for PV:WT mice. F (3, 30) = 7.73, WT-off vs. WT-on: $p = 0.9764$, WT-off vs. APP-off: $p = 0.0484$, APP-off vs. APP-on: $p = 0.0004$. **F** Sucrose preference percentage in the sucrose preference test upon optogenetic activation, $n = 10$ for PV:APP mice, $n = 7$ for PV:WT mice. F (3, 30) = 7.41, WT-off vs. WT-on: $p = 0.9758$, WT-off vs. APP-off: $p = 0.0013$, APP-off vs. APP-on: $p = 0.0376$. **G** Location of implanted optic fibers in APP and WT mice (left) and a representative image (right). **H** Schedule and diagram for the chemogenetics experiment. **I** Representative image of viral transduction and a close-up showing EGFP-positive neurons were highly localized in PV$^+$ neurons. **J** Spontaneous alternation percentage in the Y-maze test upon chemogenetic activation, $n = 9$ for each group. CNO was administrated in all groups. F (2, 24) = 9.62, WT-EGFP vs. APP-EGFP: $p = 0.0008$, APP-EGFP vs. APP-hM3D(Gq): $p = 0.0050$. **K** Immobility time in the tail suspension test upon chemogenetic activation, $n = 9$ for each group. CNO was administrated in all groups. F (2, 24) = 8.69, WT-EGFP vs. APP-EGFP: $p = 0.0026$, APP-EGFP vs. APP-hM3D(Gq): $p = 0.0027$. **L** Sucrose preference percentage in the sucrose preference test upon chemogenetic activation, $n = 9$ for each group. CNO was administrated in all groups. F (2, 24) = 9.92, WT-EGFP vs. APP-EGFP: $p = 0.0005$, APP-EGFP vs. APP-hM3D(Gq): $p = 0.0076$. Data were shown as mean ± SEM. One-way ANOVA followed by Tukey's post hoc test for **D**–**F**. One-way ANOVA followed by Dunnett's post hoc test for **J**–**L**. *$p < 0.05$, **$p < 0.01$, ***$p < 0.001$; ns no significance.

ratio in disease models [35]. It has been shown that although most synapses and neurons are excitatory in the cortex, inhibitory connectivity primarily regulates the balance of cortical network and memory pattern formation [36]. There is increasing evidence that abnormal inhibitory synaptic transmission is an important factor in AD pathogenesis at an early stage [14, 37, 38]. Our results showed that the inhibitory presynaptic release property which related short-term plasticity at GABAergic terminals is increased, and there is an E/I imbalance in the PFC of AD mice. Therefore, this E/I imbalance may be primarily due to disrupted inhibitory synaptic plasticity.

PV$^+$ INs deficits are considered a cause of GABAergic transmission impairment in the late stage of AD [20, 39, 40]. Here, we show significant deficits in GABAergic inhibitory transmission and alternations in PV$^+$ IN activity and number in the PFC in the early stage of AD in APP/PS1 mice. Our results support the notion that PV$^+$ IN deficits and E/I imbalance might be pathological mechanisms in AD. More importantly, our studies reveal that PV$^+$ INs deficits in the PFC is probably one of the earliest events in the development of AD. This is much earlier than PV$^+$ INs deficits in other brain regions including hippocampus [21, 41], which is considered one of the most vulnerable regions in AD [20]. These findings suggest that more attention should be given to PFC function in the early diagnosis of AD. Previous research has shown that amyloid β-protein (Aβ) can suppress the number and activity of GABAergic INs, resulting in abnormal network activity and cognitive impairment in AD mice [39]. Impaired activity of PV$^+$ IN in the hippocampus is detected in APP/PS1 mice at 24 weeks of age, while PV$^+$ INs in the hippocampus are initially hyperexcitable at 15–17 weeks of age or upon acute Aβ application [21]. The number of PV$^+$ INs was demonstrated to be decreased in the hippocampal CA1 and CA2 regions of 10-month-old APP/PS1 mice [41]. Our studies reveal Aβ deposition and decreased PV$^+$ INs activity and number in the PFC of 9- to 11-week-old APP/PS1 mice. Whether PV$^+$ INs are hyperactivated before amyloid plaque formation in the PFC needs further investigation.

Microcircuit in the PFC contains a complex inhibitory network, which includes multiple types of interneurons such as PV$^+$ and SST$^+$ INs [32]. These GABAergic interneurons express GAD65, GAD67 and vGAT in different levels. Some previous work showed that some PV$^+$ INs in the cortex expressed low levels of GAD65 and vGAT [42, 43]. Whether these PV$^+$ INs are more vulnerable and whether the activation of any other type of interneurons is increased (SST$^+$ INs inhibit both PV$^+$ INs and pyramidal neurons directly) in the early stage of AD and, thus, the protein levels of the GABA synthesis and transport proteins, which did not change, remain unclear and require further investigation.

It is well established that the specific α subunit composition of $GABA_A$ receptors determines the kinetics of inhibitory currents, particularly their decay time [44–46]. Previous research proved that, in recombinant $GABA_A$ receptors expressed in cultured cells, the decay time of current response after a short pulse application of GABA is faster in the receptors containing the α1 subunit compared with those containing the α2 or α3 subunits [47]. The loss of the α1 subunit leads to slower kinetics of $GABA_A$ receptors [48]. Therefore, it is possible that mIPSCs in the PFC of AD mice acquire slow decay time kinetics because of the change in the density of $GABA_A$ receptor α subunits, and our results supported this hypothesis. However, the mechanism underlying this change in the early stage of AD remains unclear and deserves further investigation. One possible reason is that PV$^+$ INs provide somatic (basket cells) and perisomatic (chandelier cells) inputs to pyramidal neurons, which show faster $GABA_A$ receptor-mediated IPSCs than distal dendritic inputs [44–47]. In addition, the synapses of PV$^+$ basket cells largely contain α1 subunits [46, 47]. These findings support that the loss of PV$^+$ INs in the PFC of AD mice caused slower mIPSC kinetics and changes in the density of α1 subunits.

Overall, our study uncovers the symptoms, including depressive-like behavior and short-term spatial memory deficits, of mice with AD at the early stage and the underlying mechanism by which PV$^+$ IN deficits cause microcircuit changes and E/I imbalance in the PFC. These early symptoms can be reversed by optogenetic or chemogenetic activation of PV$^+$ INs. These findings provide potential targets for the diagnosis and treatment of AD in the early stage.

REFERENCES

1. Germano C, Kinsella GJ. Working memory and learning in early Alzheimer's disease. Neuropsychol Rev. 2005;15:1–10.
2. Perin S, Harrington KD, Lim YY, Ellis K, Ames D, Pietrzak RH, et al. Amyloid burden and incident depressive symptoms in preclinical Alzheimer's disease. J Affect Disord. 2018;229:269–74.
3. Dafsari FS, Jessen F. Depression-an underrecognized target for prevention of dementia in Alzheimer's disease. Transl Psychiatry. 2020;10:160.
4. Teipel SJ, Wohlert A, Metzger C, Grimmer T, Sorg C, Ewers M, et al. Multicenter stability of resting state fMRI in the detection of Alzheimer's disease and amnestic MCI. NeuroImage Clin. 2017;14:183–94.
5. Pentz R, Iulita MF, Ducatenzeiler A, Bennett DA, Cuello AC. The human brain NGF metabolic pathway is impaired in the pre-clinical and clinical continuum of Alzheimers disease. Mol Psychiatry. 2021;26:6023–37.
6. Zheng Y, Liu A, Wang ZJ, Cao Q, Wang W, Lin L, et al. Inhibition of EHMT1/2 rescues synaptic and cognitive functions for Alzheimer's disease. Brain J Neurol. 2019;142:787–807.
7. Euston DR, Gruber AJ, McNaughton BL. The role of medial prefrontal cortex in memory and decision making. Neuron. 2012;76:1057–70.
8. Warden MR, Selimbeyoglu A, Mirzabekov JJ, Lo M, Thompson KR, Kim SY, et al. A prefrontal cortex-brainstem neuronal projection that controls response to behavioural challenge. Nature. 2012;492:428–32.
9. Isaacson JS, Scanziani M. How inhibition shapes cortical activity. Neuron. 2011;72:231–43.
10. Styr B, Slutsky I. Imbalance between firing homeostasis and synaptic plasticity drives early-phase Alzheimer's disease. Nat Neurosci. 2018;21:463–73.
11. Shimojo M, Takuwa H, Takado Y, Tokunaga M, Tsukamoto S, Minatohara K, et al. Selective disruption of inhibitory synapses leading to neuronal hyperexcitability

at an early stage of tau pathogenesis in a mouse model. J Neurosci Off J Soc Neurosci. 2020;40:3491–501.
12. Zádori D, Veres G, Szalárdy L, Klivényi P, Toldi J, Vécsei L. Glutamatergic dysfunctioning in Alzheimer's disease and related therapeutic targets. J Alzheimer's Dis. 2014;42:S177–87.
13. Shankar GM, Bloodgood BL, Townsend M, Walsh DM, Selkoe DJ, Sabatini BL. Natural oligomers of the Alzheimer amyloid-beta protein induce reversible synapse loss by modulating an NMDA-type glutamate receptor-dependent signaling pathway. J Neurosci Off J Soc Neurosci. 2007;27:2866–75.
14. Palop JJ, Chin J, Roberson ED, Wang J, Thwin MT, Bien-Ly N, et al. Aberrant excitatory neuronal activity and compensatory remodeling of inhibitory hippocampal circuits in mouse models of Alzheimer's disease. Neuron. 2007;55:697–711.
15. Selkoe DJ. Early network dysfunction in Alzheimer's disease. Science. 2019;365:540–41.
16. Villette V, Dutar P. GABAergic microcircuits in Alzheimer's disease models. Curr Alzheimer Res. 2017;14:30–9.
17. Shu S, Zhu H, Tang N, Chen W, Li X, Li H, et al. Selective degeneration of entorhinal-CA1 synapses in Alzheimer's disease via activation of DAPK1. J Neurosci Off J Soc Neurosci. 2016;36:10843–52.
18. DeFelipe J, López-Cruz PL, Benavides-Piccione R, Bielza C, Larrañaga P, Anderson S, et al. New insights into the classification and nomenclature of cortical GABAergic interneurons. Nat Rev Neurosci. 2013;14:202–16.
19. Hu H, Gan J, Jonas P. Interneurons. Fast-spiking, parvalbumin^{+} GABAergic interneurons: from cellular design to microcircuit function. Science. 2014;345:1255263.
20. Yang X, Yao C, Tian T, Li X, Yan H, Wu J, et al. A novel mechanism of memory loss in Alzheimer's disease mice via the degeneration of entorhinal-CA1 synapses. Mol Psychiatry. 2018;23:199–210.
21. Hijazi S, Heistek TS, Scheltens P, Neumann U, Shimshek DR, Mansvelder HD, et al. Early restoration of parvalbumin interneuron activity prevents memory loss and network hyperexcitability in a mouse model of Alzheimer's disease. Mol Psychiatry. 2020;25:3380–98.
22. Iaccarino HF, Singer AC, Martorell AJ, Rudenko A, Gao F, Gillingham TZ, et al. Gamma frequency entrainment attenuates amyloid load and modifies microglia. Nature. 2016;540:230–35.
23. Cao D, Lu H, Lewis TL, Li L. Intake of sucrose-sweetened water induces insulin resistance and exacerbates memory deficits and amyloidosis in a transgenic mouse model of Alzheimer disease. J Biol Chem. 2007;282:36275–82.
24. Kodama M, Fujioka T, Duman RS. Chronic olanzapine or fluoxetine administration increases cell proliferation in hippocampus and prefrontal cortex of adult rat. Biol Psychiatry. 2004;56:570–80.
25. Jobson DD, Hase Y, Clarkson AN, Kalaria RN. The role of the medial prefrontal cortex in cognition, ageing and dementia. Brain Commun 2021;3:fcab125.
26. Guo J, Ran M, Gao Z, Zhang X, Wang D, Li H, et al. Cell-type-specific imaging of neurotransmission reveals a disrupted excitatory-inhibitory cortical network in isoflurane anaesthesia. EBioMedicine. 2021;65:103272.
27. Chen J, Shu S, Chen Y, Liu Z, Yu L, Yang L, et al. AIM2 deletion promotes neuroplasticity and spatial memory of mice. Brain Res Bull. 2019;152:85–94.
28. Liu Y, Bian H, Xu S, Shu S, Jia J, Chen J, et al. Muscone ameliorates synaptic dysfunction and cognitive deficits in APP/PS1 mice. J Alzheimer's Dis. 2020;76:491–504.
29. Tan Z, Robinson HL, Yin D-M, Liu Y, Liu F, Wang H, et al. Dynamic ErbB4 activity in hippocampal-prefrontal synchrony and top-down attention in rodents. Neuron. 2018;98:380–93.e4.
30. Kasugai Y, Vogel E, Hörtnagl H, Schönherr S, Paradiso E, Hauschild M, et al. Structural and functional remodeling of amygdala GABAergic synapses in associative fear learning. Neuron. 2019;104:781–94.
31. Ghosal S, Hare B, Duman RS. Prefrontal cortex GABAergic deficits and circuit dysfunction in the pathophysiology and treatment of chronic stress and depression. Curr Opin Behav Sci. 2017;14:1–8.
32. Wonders CP, Anderson SA. The origin and specification of cortical interneurons. Nat Rev Neurosci. 2006;7:687–96.
33. Tyson JA, Anderson SA. GABAergic interneuron transplants to study development and treat disease. Trends Neurosci. 2014;37:169–77.
34. Bartley AF, Dobrunz LE. Short-term plasticity regulates the excitation/inhibition ratio and the temporal window for spike integration in CA1 pyramidal cells. Eur J Neurosci. 2015;41:1402–15.
35. Chen L, Li X, Tjia M, Thapliyal S. Homeostatic plasticity and excitation-inhibition balance: the good, the bad, and the ugly. Curr Opin Neurobiol. 2022;75:102553.
36. Mongillo G, Rumpel S, Loewenstein Y. Inhibitory connectivity defines the realm of excitatory plasticity. Nat Neurosci. 2018;21:1463–70.
37. Kiss E, Gorgas K, Schlicksupp A, Groß D, Kins S, Kirsch J, et al. Biphasic alteration of the inhibitory synapse scaffold protein gephyrin in early and late stages of an Alzheimer disease model. Am J Pathol. 2016;186:2279–91.
38. Busche MA, Kekuš M, Adelsberger H, Noda T, Förstl H, Nelken I, et al. Rescue of long-range circuit dysfunction in Alzheimer's disease models. Nat Neurosci. 2015;18:1623–30.
39. Verret L, Mann EO, Hang GB, Barth AM, Cobos I, Ho K, et al. Inhibitory interneuron deficit links altered network activity and cognitive dysfunction in Alzheimer model. Cell. 2012;149:708–21.
40. Martinez-Losa M, Tracy TE, Ma K, Verret L, Clemente-Perez A, Khan AS, et al. Nav1.1-overexpressing interneuron transplants restore brain rhythms and cognition in a mouse model of Alzheimer's disease. Neuron. 2018;98:75–89.
41. Takahashi H, Brasnjevic I, Rutten BP, Van Der Kolk N, Perl DP, Bouras C, et al. Hippocampal interneuron loss in an APP/PS1 double mutant mouse and in Alzheimer's disease. Brain Struct Funct. 2010;214:145–60.
42. Hioki H, Okamoto S, Konno M, Kameda H, Sohn J, Kuramoto E, et al. Cell type-specific inhibitory inputs to dendritic and somatic compartments of parvalbumin-expressing neocortical interneuron. J Neurosci Off J Soc Neurosci. 2013;33:544–55.
43. Fish KN, Rocco BR, Lewis DA. Laminar distribution of subsets of GABAergic axon terminals in human prefrontal cortex. Front Neuroanat. 2018;12:9.
44. Miles R, Tóth K, Gulyás AI, Hájos N, Freund TF. Differences between somatic and dendritic inhibition in the hippocampus. Neuron. 1996;16:815–23.
45. Soltesz I, Smetters DK, Mody I. Tonic inhibition originates from synapses close to the soma. Neuron. 1995;14:1273–83.
46. Lewis DA, Fish KN, Arion D, Gonzalez-Burgos G. Perisomatic inhibition and cortical circuit dysfunction in schizophrenia. Curr Opin Neurobiol. 2011;21:866–72.
47. Freund TF. Interneuron diversity series: rhythm and mood in perisomatic inhibition. Trends Neurosci. 2003;26:489–95.
48. Goldstein PA, Elsen FP, Ying SW, Ferguson C, Homanics GE, Harrison NL. Prolongation of hippocampal miniature inhibitory postsynaptic currents in mice lacking the GABA(A) receptor alpha1 subunit. J Neurophysiol. 2002;88:3208-17.

ACKNOWLEDGEMENTS

We appreciate PV-Cre mice support by Professor Ji Hu from ShanghaiTech University.

AUTHOR CONTRIBUTIONS

YX and SS initiated, designed the study and wrote the manuscript. SS and S-YX performed the electrophysiological experiments and animal experiments, and analyzed the data. LY, YL, XC and X-LZ performed molecular biological experiments. J-QJ and H-JB collected the interstitial fluid samples. YL performed virus injection experiments. All authors approved the manuscript prior to submission.

FUNDING

This work was supported by grants from the National Natural Science Foundation of China (Nos. 81901091, 81630028 and 81920108017), the Natural Science Foundation of Jiangsu Province of China (BK20190124), the China Postdoctoral Science Foundation (No. 2019M651806), the Key Research and Development Program of Jiangsu Province of China (No. BE2020620) and Jiangsu Province Key Medical Discipline (ZDXKA2016020).

COMPETING INTERESTS

The authors declare no competing interests.

ADDITIONAL INFORMATION

Supplementary information The online version contains supplementary material available at https://doi.org/10.1038/s41386-022-01435-w.

Correspondence and requests for materials should be addressed to Yun Xu.

Reprints and permission information is available at http://www.nature.com/reprints

Publisher's note Springer Nature remains neutral with regard to jurisdictional claims in published maps and institutional affiliations.